A Computational Investigation: The Influence of Group-6 Organometallic Chelates on C-H Bond Activation and Methane-to-Methanol Oxidation Cycles

Abstract

Despite advances in the petrochemical field since the 1960's, a commercially viable catalyst for the oxidization of light alkanes has yet to be found. Our research investigates the effects of various metal complexes in functionalizing the inert C-H bond of methane. Structured after the α-subunit of the enzyme ethylbenzene dehydrogenase, we proposed a promising organometallic complex in the form of $[M(L_C)_2(L_T)O]^{-1}$ (L_C = ethylene-dithiolate, cis-2,3-butylene-dithiolate; L_T = H, OH, NO_3, CN; M= Mo^{VI}, Cr^{VI}, W^{VI}), with further investigation into the prospective role of ammonium as a key charge-balancing proton-donor. Conducted using Density-Functional Theory (DFT) methods, this study found Cr-based catalysts as most adept in hydrogen atom abstraction from methane by at least ~20 kcal mol^{-1} in comparison to Mo- and W-based catalysts. Evaluation of ammonium involvement across all reaction coordinates revealed a universal preference for intermediate ammonium pathways, while reactant ammonium adduct formation varied case-by-case. Analysis of average differences in relative free energies revealed small trans ligand influence on catalyst performance, and additional analysis of ethylene-dithiolate C-C bond lengths throughout the reaction coordinate revealed the innocence of the bidentate cis ligands. Overall, this study emphasizes the vast potential of six-coordinate Cr-based metal catalysts in lowering the C-H activation barrier.

I. INTRODUCTION

The development of an economically viable catalyst for direct conversion of methane to methanol has long been a "Holy Grail" of hydrocarbon catalysis [1, 3]. As environmental concerns rise, an alternative, liquid energy source that minimizes environmental impacts while still satisfying global energy requirements is very desirable. Methane, the primary ingredient in natural gas, yields more heat per mass (15.21 kWh per kg) and less carbon dioxide per unit of heat released (0.55 kg per kWh) than any other fossil fuel [2, 16]. Despite its abundance and chemical simplicity, however, methane falls short of being a desirable fossil fuel due to its low energy density by volume; transportation of the gas is only feasible by compression, an expensive process [2]. Thus, development of a methane to methanol (MTM) catalytic conversion cycle becomes increasingly important. This study investigates one such methane-to-methanol cycle via a promising catalyst structure inspired by a newly-characterized enzyme.

Methanol (CH_3OH) is appealing not just because it bypasses methane's transportation challenges: its economic advantages potentially surpass even those of other common alternative energy sources (e.g., hydrogen, nuclear, solar, hydroelectric, etc.), as current commercial infrastructure favors the transportation and storage of liquids [3, 4]. Serving as an efficient means of storing and transporting energy, methanol finds equal use as both a high-energy density transportation fuel and a chemical feedstock [3-5]. As described by Olah, the potential for a "methanol economy" is immense should science develop a sustainable manufacturing process for this chemical [4].

At present, methanol generation involves a highly expensive and energy-inefficient two-step process, whereby methane is first broken down into a CO/H_2 hybrid (syngas), then reassembled into methanol via transition metal catalysts [3-5]. The syngas detour step is very

endothermic and thus incredibly energy intensive [3-5]. A more economical approach would be to directly generate methanol from methane by a single-step, low temperature process. Because the gas-phase oxidation of methane is exothermic, methane is viable for oxidation by a variety of oxidants [1, 2]. Therefore, exploring possible catalysts for a direct methane-to-methanol oxidation cycle has been a large focus of recent research [3-6]. The primary challenges of achieving low temperature, high yield partial oxidation of methane lies in the difficulties of selectively functionalizing the C-H bond of interest, in addition to recovering the products of oxidation before they go further down the oxidation cascade [6]. These obstacles arise because of two main reasons: the relative inertness of alkane C-H bonds [2] and the higher reactivity of the oxidized products compared to their alkane reactants [6]. Previous literature suggests that Pt-based Shilov-system catalysts [20] and Hg-based catalysts [12] result in the highest yield and most favorable selectivity of methane or similar derivatives. Drawbacks of these systems that inhibit them from commercial use, however, include the high price of the metals, the tendency to produce undesirable side products, inhibition by water, and difficulty recovering and recycling the catalysts after use [1-3, 7, 10].

It is here that ethylbenzene dehydrogenase, an enzyme found in denitrifying bacteria strains, became particularly relevant to hydrocarbon catalysis. Ethylbenzene dehydrogenase (EDBH), a recently characterized enzyme, is capable of anaerobically catalyzing the oxidation of higher hydrocarbons, such as ethylbenzene, into alcohols [8, 21-23]. As found in nature, the enzyme oxidizes ethylbenzene to (S)-1-phenylethanol [21-23]. Drawing similarities between EDBH's role in direct hydrocarbon oxidation and our goal of direct methane-to-methanol oxidation, we modeled our suggested catalyst after a cofactor in the α-subunit of EDBH.

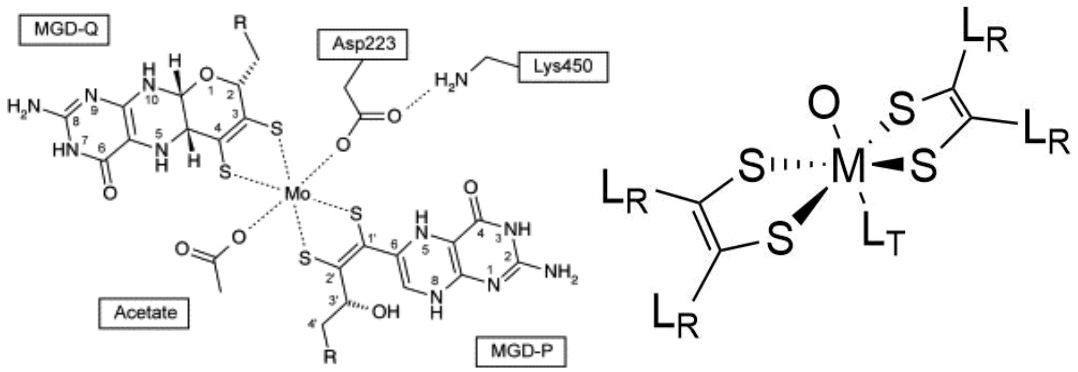

Figure 1.2 A side-by-side comparison of a cofactor from the α-subunit of EDBH [23] (left) and our catalyst structure (right), with L_R = H, CH_3 and L_T = F, OH, NO_3, CN.

In our investigation, we proposed a non-precious metal-based organometallic complex in the form of $[M(L_C)_2(L_T)O]^{-1}$ (L_C = ethylene-dithiolate, cis-2,3-butylene-dithiolate; L_T = H, OH, NO_3, CN; M= Mo^{VI}, Cr^{VI}, W^{VI}) as a catalyst, where L_C represents the bidentate cis ligand, M represents the metal center, and L_T represents the trans ligand. Totaling 24 possible combinations of metals and ligands, each unique structure represents a corresponding possible reaction system. In this study, we successfully modeled the electronic structures of each system, deriving key information such as vibrational frequencies, ligand bond lengths, and changes in enthalpy (ΔH) and Gibbs free energy (ΔG), which we then used to draw conclusions about how each reaction cycle behaved.

Each reaction begins with an oxo-active species that proceeds to activate methane through a hydrogen atom abstraction (HAA) pathway. The primary focus of this study is defining the HAA activation barrier of each reaction, obtained through taking the change in free energy between the oxo-active species, the methane substrate, and the HAA transition state. Put in other terms, we look to compare the kinetic ease of each reaction, which is very important in gauging a proposed catalyst's suitability in methanol production. To ascertain the more favored electronic state, we defined two possible spin multiplicities for each HAA transition state: singlet and triplet. A unique point of interest we investigated, however, was how a proton-donor might alter reaction behavior.

In summing the oxidation states of ligands, center metals, and oxygen active sites, we realized our complex had a net anionic charge of 1-. We then sought to investigate the influence a charge balancer, in our case an ammonium, would have on reaction mechanisms and favorability. Thus, in addition to the metal catalyst and methane reactants, we introduced a third reagent, ammonium (NH_4), and investigated possible adduct pathways and Brønsted-Lowry acid-base interactions between it and our complex. To close the catalytic cycle after the methanol dissociates from the system, the active species, having donated its oxygen to oxidize methane, is regenerated via an oxygen atom transfer step [3, 11]. This study focuses exclusively on the C-H activation of methane and subsequent oxidation into methanol, with emphasis on the influence of center metals, cis/trans ligands, and an ammonium base additive.

II. DESCRIPTION OF RESEARCH

A. Defining Reaction Mechanisms and Catalyst Structure

The methane-to-methanol reactions that we aimed to evaluate consist of four critical steps starting from the initial reactants (CH_4, NH_4^+, oxo): C-H activation followed by a hydrogen atom abstraction (HAA) from CH_4 to form some combination of the hydrogenated complex, ammonium or ammonia, and a methyl radical; a radical rebound (RR) to form a methanol adduct and ammonium; methanol dissociation from the metal; and catalysis regeneration via oxygen atom transfer. We modeled these steps as stationary points throughout the reaction coordinate, each point consisting of a sum of the reactants, intermediates, or products of each step. Our research mainly focuses on the energy barrier of the C-H activation of methane ($\Delta G^{\ddagger}$), as it is the proposed rate determining step [12]. In detail, this step involves the breaking of a C-H methane bond and the subsequent transfer of the hydrogen to the oxo, forming a hydroxyl group. We characterized this energy barrier by building a plausible transition state guess that lay between our reactants and

HAA intermediates, performing a DFT optimization, and then calculating $\Delta G^{\ddagger}$ by evaluating the resulting output molecule.

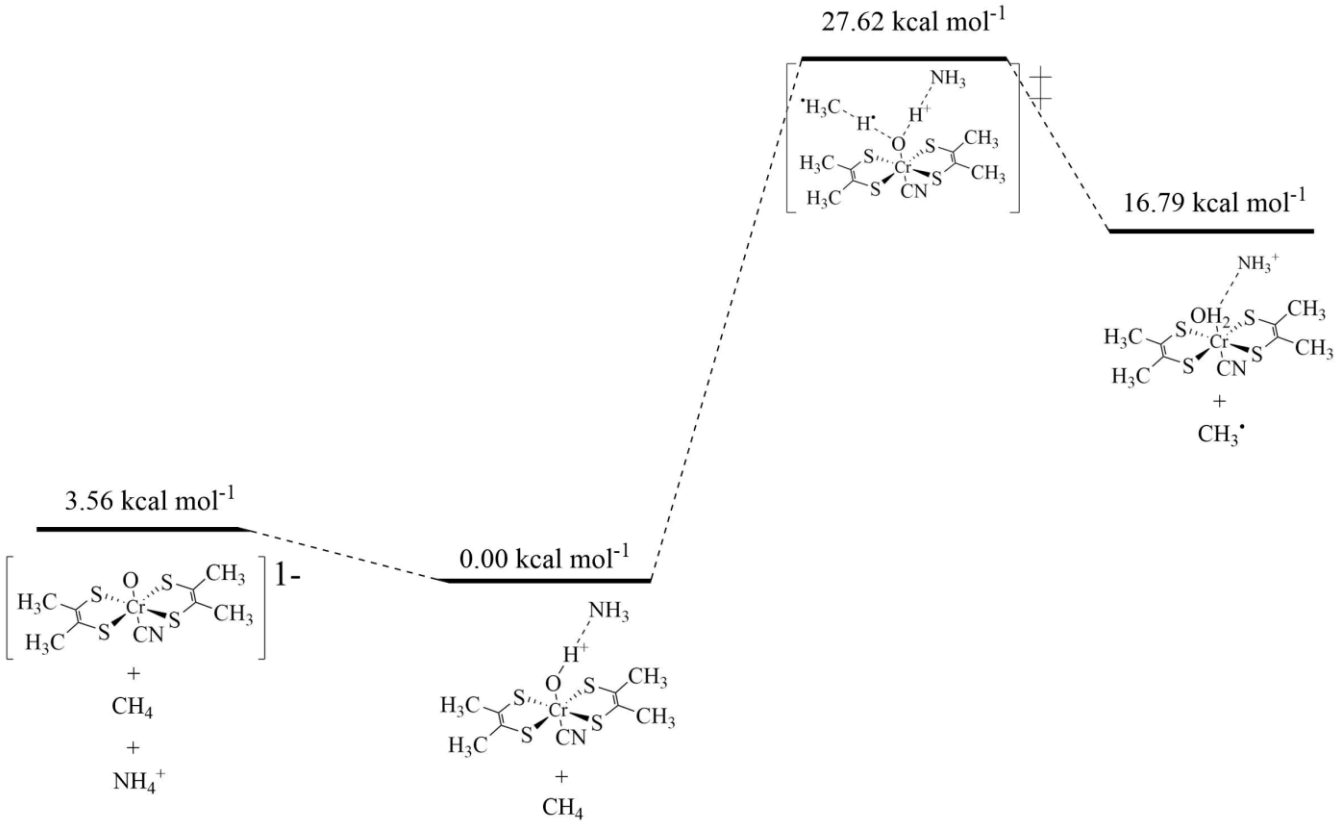

Figure 2.1. An example of the activation energy barrier of the C-H activation mechanism. The characterized reaction (M=Cr; L_C = cis-2,3-butylene-dithiolate; L_T = CN) includes ammonium adduct formation before and after the transition state. ΔG is calculated relative to the zero point of our reactants, which we took in this reaction to be the ammonium adduct pathway

One of the most crucial aspects of this study involves the minimization of $\Delta G^{\ddagger}$, the relative free energy of transition states. We proposed variations of a catalyst structure inspired by a cofactor of EDBH in the hopes of replicating its efficient hydrocarbon oxidation. The original cofactor structure is six-coordinate, with a molybdenum (Mo) center, two dithiolene groups as cis ligands with each bonded twice to the center metal, and Asp223-Oδ2 and acetate occupying the fifth and sixth ligand bonds [23]. With this structure in mind, we first chose to investigate the effects of replacing the center Mo with chromium (Cr) and tungsten (W), two similar Group-6 transition

metals. Because of these atoms' similar electronic properties, it became interesting to see how Cr, Mo, and W would vary in catalyst favorability.

As for the ligands attached to the metal ion, we investigated two variations of R-groups on the ethylene-dithiolate cis ligand: hydride (H^-) and methyl (CH_3^-) as well as four variations on the trans ligand: hydroxide (OH^-), fluoride (F^-), cyanide (CN^-), and nitrate (NO_3^-). We purposely picked a mixture of known strong, neutral, and weak trans effect ligands ($F^- < OH^- < H^- < CN^-$) [24], investigating how these ligands might alter the catalyst rate. As for our cis ligand, previous literature characterizes the cis effect as prominent in octahedral metal complexes, especially anionic ones [29]. Thus, we opted for two anionic R-groups: H^- and CH_3^-. Our project places a greater emphasis on the consequences of varying our trans ligand and center metal than the consequences of varying our cis ligand, as literature precedent provides a strong foundation for dithiolene cis ligand effects [29, 30]. Overall, the combinations of the central metal along with the cis and trans ligand variations make up 24 distinct active species models. Our project aims to determine the best performing model in activating the inert C-H bond of methane.

B. Computational Methods and the Process of Achieving Convergence

To create and properly examine the molecules that we theorized would catalyze the reaction process, we used 3D-modeling and visualization software in the form of GaussView [25] and Chemcraft [26]. In GaussView, we built our initial molecule guess structures, resulting in a rough initial geometry that we cleaned and optimized through DFT calculations. We based all data and conclusions off DFT-optimized systems, which represent either the ground state or true transition state of our systems.

We specified in our DFT calculation inputs for an optimization of molecular geometry and an analysis of our frequency and thermochemistry, with all computational methods based on

literature precedent, which suggested our calculation specifications to be the most experimentally accurate [3, 13-15]. We performed all calculations with the Gaussian09 package [17] at the B97D/6-31+G(d) level of theory [18], with reactions simulated in an acetonitrile solvent, a polar solvent, by the SMD continuum solvation model [19] to stabilize anion and cation behavior. Our jobs specifically involved density functional theory (DFT) to approximate solutions to the Schrödinger equation of our systems [31]. These methods assume certain parameters for the system and work off these parameters to arrive at a solution, which communicates information about a system's electronic behavior, structure, and thermochemistry. By extracting key data points concerning electronic and thermodynamic properties of interest, we can then draw conclusions on the favorability of our various metal complexes.

Other calculation specifications include free energies as calculated by Gaussian, given in Hartrees; we convert and report these in kcal mol^{-1}. Ground state systems are local minima marked by no imaginary frequencies, while transition states are local maxima containing exactly one imaginary frequency corresponding to the reaction of interest.

As we used DFT to optimize distinct molecular geometries, we encountered errors with the program that occurred for several reasons. These include but are not limited to incorrect textual input data files, imperfect geometric symmetry in molecular point groups, incomplete basis sets, and, in general, a misconstrued initial guess structure. Particularly, one such convergence error resulted from an intrinsic limitation of DFT methods in calculating unstable chemical bonding situations [31]. To correct these errors, we often had to tighten calculation parameters or reconstruct our model of the system.

For transition states, specifically, our convergence criteria had to be especially strict because locating these states usually involves optimizing the active bond to a local maximum while

forcing the rest of the bond lengths/angles down to local minima. Compared to the straight optimization of a non-transition state system to a ground state, transition states are more numerically sensitive and take more time to calculate. To achieve this level of accuracy, we continuously modified second derivative (force constants and frequencies) calculation criteria, which was either calculated initially by Gaussian and then approximated in further steps (Opt=CalcFC), or re-calculated at each step (Opt=CalcAll). Approximating the force constants was usually enough, though we turned to a detailed re-calculation of force constants at each step for particularly difficult optimizations, albeit at the expense of computational resources and time. Using the ModRedundant function, we also isolated the minima and maxima optimizations by freezing the active bond(s) of interest and forcing a minimization of the surrounding system, then unfreezing the active bond and optimizing the structure again to a local maximum. Monitoring the average root mean squared (RMS) of the forces in our system at every step of the reaction cycle was also helpful in resolving calculation errors. RMS forces lower as the calculation approaches convergence; recording this property allowed us to reevaluate molecules using the lowest average RMS step as our initial guess for future iterations of our calculations.

C. Influence of Ammonium Additives

In the interest of further increasing catalyst favorability, a point of interest for our project included the effects a proton-donor might have on the reaction mechanisms and favorability. We introduced ammonium as a third reagent, seeking to investigate its role as a charge-balancer and weak Brønsted-Lowry based acid. The reactions began with the oxo active species reacting with methane and ammonium ($[M(L_C)_2(L_T)O]^{-1}$ + CH_4 + NH_4^+). We discovered initial ammonium adduct formations in some reaction cycles (Table 2.1). Thus, two reactant possibilities emerged: the reactants stay as three separate entities, or the ammonium forms an adduct with the oxo through

hydrogen bonding. For reactions pathways where an adduct was discovered, we investigated tautomer orientations as well. For calculation of relative free energies of points further along the reaction coordinate, we considered the most favored reactant pathway as the zero point.

	R-Group of Cis Trans	H OH	H CN	H F	H NO_3	CH_3 OH	CH_3 CN	CH_3 F	CH_3 NO_3
Cr	Initial Pathway	Separate	Separate	Separate	Separate	Oxo-Add.	Oxo-Add.	Separate	Separate
Cr	Δ Kcal/mol	2.1	3.0	6.8	3.4	-6.8	-3.6	3.2	5.4
Cr	HAA Pathway	Aqua Cplx.	Oxo-Add.	Aqua Cplx.	NH_4-Add.	Oxo-Add.	Oxo-Add.	NH_4-Add.	NH_4-Add.
Cr	Δ Kcal/mol	-4.7	-0.1	-2.2	-5.7	-10.5	-8.5	-8.8	-7.1
Mo	Initial Pathway	Separate	Separate	NH_4-Add.	Separate	Oxo-Add.	Separate	NH_4-Add.	Oxo-Add.
Mo	Δ Kcals/mol	10.0	11.8	-3.2	1.5	-17.7	0.6	-4.0	-8.0
Mo	HAA Pathway	Oxo-Add.	Oxo-Add.	Oxo-Add.	NH_4-Add.	NH_4-Add.	NH_4-Add.	Oxo-Add.	Oxo-Add.
Mo	Δ Kcals/mol	-2.7	-1.8	-1.1	-0.2	-9.5	-4.5	-4.6	-1.0
W	Initial Pathway	Separate	Oxo-Add.	Oxo-Add.	Separate	Oxo-Add.	Separate	Oxo-Add.	Oxo-Add.
W	Δ Kcals/mol	12.1	-14.6	-4.6	0.4	-1.9	0.9	-4.3	-0.9
W	HAA Pathway	Oxo-Add.	Oxo-Add.	Oxo-Add.	Oxo-Add.	Oxo-Add.	Oxo-Add.	Oxo-Add.	Aqua Cplx.
W	Δ Kcals/mol	-4.4	-0.7	-0.8	-0.0	-4.4	-0.3	-3.3	-14.6

Table 2.1. A collection of relative free energies and preferred reaction pathways for reactants and HAA intermediates given the introduction of ammonium. In the case an adduct was discovered, tautomer orientation was also investigated and reported as either oxo-leaning or NH_4-leaning. Free energies of reactants are calculated relative to the more preferred pathway, while free energies of intermediates are calculated relative to an ammonium-absent reaction pathway. All free energies are reported in kcal mol^{-1}.

Following the HAA transition state, we noted three possible pathways for the HAA intermediate, each with varying degrees of ammonium deprotonation: no donation with ammonium as a spectator of the hydroxo and methyl radical, partial donation through a hydrogen-bonded adduct between the ammonium and hydroxo, and complete donation to form ammonia and an aqua complex. It is important to note that partial or complete deprotonation of ammonium neutralized the charge of the reactant complex, which was anionic.

As reported in Table 2.1, relative free energies for ammonium-involved pathways were lower than ammonium-absent pathways for every HAA intermediate pathway, while ammonium-involved pathways for reactants varied case-by-case. Although we observed no discernable correlation between ammonium-involved pathways and cis/trans ligands combinations, there seems to be a general tendency towards ammonium-involved pathways as we increase the weight

of the center metal. Thus, for all reactions, including transition states, we considered the involvement of ammonium as the third reagent.

D. Geometries, Spin States, and Frequencies of HAA Transition States

	R-Group of Cis Trans	H OH	H CN	H F	H NO_3	CH_3 OH	CH_3 CN	CH_3 F	CH_3 NO_3
Cr	Δ G	33.3	30.5	33.7	42.3	32.9	27.6	31.4	47.7
Cr	Singlet/Triplet	Singlet	Singlet	Triplet	Triplet	Triplet	Triplet	Triplet	Singlet
Cr	i. frequency	-1151.3	-1404.6	-1180.4	-1214.6	-1317.6	-1183.0	-1144.9	-1286.8
Mo	Δ G	56.8	44.9	50.4	60.7	61.9	43.9	59.8	60.4
Mo	Singlet/Triplet	Singlet	Triplet	Singlet	Singlet	Singlet	Triplet	Singlet	Triplet
Mo	i. frequency	-513.3	-1391.9	-1243.0	-354.0	-1375.2	-1183.0	-335.4	-459.2
W	Δ G	65.0	63.9	55.9	53.9	75.7	50.8	64.2	55.6
W	Singlet/Triplet	Singlet	Singlet	Triplet	Triplet	Singlet	Singlet	Singlet	Triplet
W	HAA Pathway	-769.7	-915.3	-1041.5	-823.6	-235.6	-820.3	-371.6	-581.5

Table 2.2. Calculated relative free energies, spin states, and imaginary frequencies for the transition states of each reaction. Combinations of the R-group of the ethylene-dithiolate cis ligand and the trans ligand are listed as columns, while metals are listed as rows. All free energies are reported in kcal mol^{-1}.

The proposed rate determining step of this reaction is the energy barrier of activating the inert C-H bond of methane [12]; the change in free energy of our transition states in relation to our zero points characterizes this barrier. The primary focus of this study is in the influence of $[M(L_C)_2(L_T)O]^{-1}$ complexes, based on a cofactor of EDBH with a similar function, on catalyzing the activation of this bond.

Table 2.2 reports the relative free energies, spin multiplicities, and vibrational frequencies of each transition state investigated. Due to the electron configuration of our complexes, we investigated free energies for both singlet and triplet spin multiplicities: reported free energies correspond to the preferred singlet or triplet, which is labeled in Table 2.2.

Comparing quantitative trends, Cr-based catalysts possess a much lower C-H activation barrier than the Mo-based and W-based catalysts (Table 2.2). C-H activation via HAA for Cr-based transition states has an average $\Delta G^{\ddagger}$ of 35 kcal mol $^{-1}$, Mo-based transition states have an average $\Delta G^{\ddagger}$ of 55 kcal mol^{-1}, and W-based reactions have an average $\Delta G^{\ddagger}$ of 61 kcal mol^{-1}. We

calculated the [Cr(cis-2,3-butylene-dithiolate)$_2$(CN)] triplet to be 48 kcal mol^{-1} lower in free energy than the [W(cis-2,3-butylene-dithiolate)$_2$(OH)] singlet; this was the greatest free energy difference we observed.

While the central metal of the complex had a substantial impact on relative free energies, the cis and trans ligands had a less pronounced effect. In comparing the effects of H and CH_3 cis ligand R-groups on Cr-based transition states, we found no noticeable difference, with an average difference of 0.04 kcal mol^{-1} between the two. Mo-based and W-based transition states followed similar trends of minimal cis ligand impact, with an average difference of 3 kcal mol^{-1} for Mo-based transition states and 2 kcal mol^{-1} for W-based transition states. For trans ligand effects, L_T = NO_3 of Cr-based and W-based transition states seems to result in the highest free energy barrier, while L_T = CN results in the lowest relative free energy barrier. This trend disappears for W-based transition states, where L_T = OH results in the highest free energy barrier instead. Overall, observed trends for metal, cis, and trans influence point to the [Cr(cis-2,3-butylene-dithiolate)$_2$(CN)] complex to possess the lowest barrier among all modeled reactions.

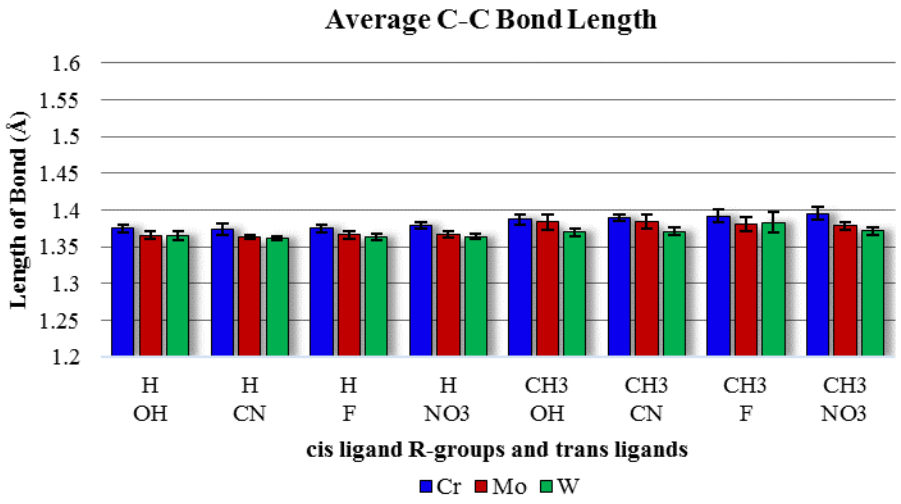

Figure 2.2. A comparison of average C-C bond lengths on bidentate cis ligand, including standard error on the mean. All standard errors were within <1%.

Because the relative free energy results imply innocence of cis ligands, we measured the C-C bonds of our ethylene-dithiolate and cis-2,3-butylene-dithiolate ligands to confirm their oxidation states throughout the reaction coordinate. Figure 2.2 shows the average of each C-C bond for each catalyst reaction. Taken across all stationary points including transition states, the length of these C-C bonds helped us determine the redox oxidation state of the cis ligand and whether it changed or remained constant across the reaction coordinate. Because the measured C-C bond length, approximately ~1.38 Å, remained constant regardless of catalyst structure or reaction step, we concluded that our cis ligands are redox innocent, which corroborates with their impact on relative free energy.

$$\bar{\nu} = \frac{1}{2\pi c}\sqrt{\frac{k}{\mu}}.$$

Equation 2.1. Equation for the vibrational frequency of a group of atoms, where c and k are constants and μ is the total mass of the oscillating atoms [32].

A single imaginary frequency corresponding to the active bond of interest characterizes each transition state. In this reaction, imaginary frequencies correspond to a methane hydrogen atom oscillating between the methyl radical and oxygen active site of the oxo. These frequencies, imaginary or otherwise, are considered simple harmonic oscillators and are represented by Equation 2.1. Because mass is inversely proportional to frequency, either a greater number of vibrating atoms or more massive atoms will lower the overall vibrational frequency for a given force constant (k). For our transition states, we expected the ideal vibrational frequency to correspond with the oscillating hydrogen and be around 1000i cm^{-1}, given the small mass of a hydrogen atom. However, realistically such a frequency only appeared in the most well-behaved of transition states, such as the [Cr(cis-2,3-butylene-dithiolate)$_2$(CN)] reaction. In transition states

with lower vibrational frequencies, we observed larger atom groups such as a methyl or sulfur ligand oscillating alongside the methane hydrogen. Transition states with vibrational frequencies less than 1000i cm^{-1} had considerably more difficulty abstracting the hydrogen from methane than did their >1000i cm^{-1} counterparts (Table 2.1). Thus, we found an inverse correlation between imaginary frequency and free energy barrier of transition states.

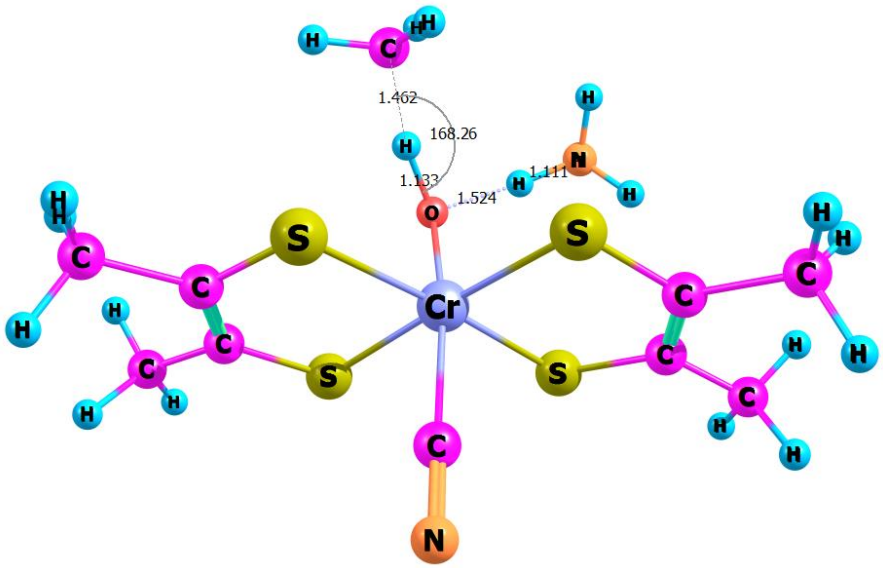

Figure 2.3. Pictured is the triplet [Cr(cis-2,3-butylene-dithiolate)$_2$(CN)] complex transition state, optimized to B97D/6-31+G(d/SMD-acetonitrile. The bond length of the oscillating C-H bond of CH_4 is shown for emphasis. Shown are the angle, O-H bond length, and bond lengths between the O and NH_4 to illustrate adduct formation. We report bond lengths in Å, while angles are in °.

E. Radical Rebound and Methanol Dissociation

For the RR and methanol disassociation, trends of Cr-based catalyst favorability continue: analysis of RR relative free energies revealed similar trends of considerably lower Cr-based catalyst reactions in comparison to Mo-based and W-based catalyst reactions (Table 2.3). Though methanol adduct formation via radical rebound for both reactions is still endergonic, Cr-based reactions are significantly less so, averaging a 28 kcal mol^{-1} lower reactant-intermediate change in Gibbs free energy compared to W-based catalyst reactions, the most thermodynamically expensive of the three metals investigated. This translates to a significantly more thermodynamically-favored

progression of reactants to methanol adduct through Cr-based catalysts than Mo-based and W-based ones.

	R-Group of Cis Trans	H OH	H CN	H F	H NO_3	CH_3 OH	CH_3 CN	CH_3 F	CH_3 NO_3
Cr	RR Δ G	5.1	11.8	10.7	28.7	7.9	4.9	8.4	28.1
Cr	MeOH Δ G	-2.4	1.3	3.9	16.9	3.1	11.9	3.9	22.5
Mo	RR Δ G	21.6	18.7	19.1	27.1	23.2	22.9	17.5	37.5
Mo	MeOH Δ G	15.4	12.2	11.2	14.8	18.1	13.2	13.1	23.4
W	RR Δ G	36.1	47.5	36.6	37.6	35.3	34.3	37.9	40.8
W	MeOH Δ G	30.9	39.7	25.0	26.4	32.0	24.7	26.2	28.4

Table 2.3. Relative free energies for the RR and methanol disassociation steps of the reaction coordinate. All free energies are reported in kcal mol^{-1}.

For the final step, the methanol must disassociate from the metal complex to permit catalyst regeneration for future cycles. The gap between Cr-based and Mo-based catalyst reactions narrows, with the range of Mo-based relative free energies overlapping with that of Cr-based catalyst reactions (Table 2.3). W-based reactions remain highly unfavorable (Table 2.3).

F. Statistical Analysis

To make sure that our data was significant, we used a variety of statistical methods and tests to validate our data. This process was necessary to prove that the trends and influential factors analyzed throughout this investigation exist mathematically. SPSS and Microsoft Excel, the software used to run these calculations, provided results from a two-way analysis of variance (ANOVA) without replication as well as a post-hoc analysis (Tukey Honest Significant Difference). These methods included descriptive statistics and comparisons of the influence our metal center had on catalyst performance versus the influence of cis and trans ligands.

Tests of Between-Subjects Effects

Dependent Variable: Gibbs_Free_Energy_of_HAA_Transition_States

Source	Type III Sum of Squares	df	Mean Square	F	Sig.	Partial Eta Squared
Corrected Model	3466.362[a]	9	385.151	8.816	.000	.850
Intercept	60124.869	1	60124.869	1376.247	.000	.990
Center_Metals	2888.608	2	1444.304	33.060	.000	.825
Cis_and_Trans_Ligands	577.754	7	82.536	1.889	.147	.486
Error	611.626	14	43.688			
Total	64202.856	24				
Corrected Total	4077.987	23				

a. R Squared = .850 (Adjusted R Squared = .754)

Table 2.4. The table above shows the Test of Between-Subjects Effects comparing the influence of center metals versus cis/trans ligands. This chart highlights the significance of their effects on the HAA transition state energies.

We originally sought out to apply three sets of t-tests to compare the influence of varying the center metal by averaging the data from all the various ligands combinations by metal. However, further research showed that this would increase the probability of a Type I error from a standard 5% to 14.3% [27], which would induce a large degree of variability within our statistical results. Therefore, we used an ANOVA to keep the Type I error at five percent. Unlike its t-test counterpart, ANOVA without replication can analyze the comparison between more than two groups (i.e. our three main metal complexes) and incorporate more than one independent variable into its analysis. Through this process, we could examine the effect of both the center molecule and the impact the cis and trans ligands had on the relative Gibbs free energy of the experimental chelate. As a precursor to running the test, we checked to see that our data fit the under lying assumptions of ANOVA which requires there to be homogeneity of variances, independence of observations, and normal distributions among the three groups. Our results rejected the null hypothesis for this statistical test which was $H_0 = \mu_1 = \mu_2 = \mu_3$ with $\alpha = 0.05$ where μ equals eight

different combinations of chelates, each with a distinct meal complex. In other terms, at least one pair of data in the three sets was statistically significant with a 95% confidence interval.

Gibbs Free Energy of HAA Transition States

Tukey HSD[a,b]

Center Metals	N	Subset 1	Subset 2
Chromium	8	34.9267	
Molybdenum	8		54.6217
Tungsten	8		60.6076
Sig.		1.0000	.202

Means for groups in homogeneous subsets are displayed.
Based on observed means.
The error term is Mean Square(Error) = 43.688.

a. Uses Harmonic Mean Sample Size = 8.000.

b. Alpha = .05.

Gibbs Free Energy of HAA Transition States

Tukey HSD[a,b]

Cis_and_Trans_Ligands	N	Subset 1
CH3CN	3	40.7549
HCN	3	45.8457
HF	3	46.6485
HOH	3	51.6763
CH3F	3	51.8156
HNO3	3	52.2841
CH3NO3	3	54.5904
CH3OH	3	56.8005
Sig.		.130

Means for groups in homogeneous subsets are displayed.
Based on observed means.
The error term is Mean Square(Error) = 43.688.

a. Uses Harmonic Mean Sample Size = 3.000.

b. Alpha = .05.

Table 2.5. The figure on the left shows statistics from the Tukey HSD analyzing the center molecules into different subsets based on data significance. Similarly, the figure on the right shows the cis and trans ligands in scope of how significantly different their data is.

Simple main effects analysis of the influence of the center molecule and the ligands seen in Table 2.4 showed that the metal had a significant impact on the Gibbs free energy of the HAA transition states (p-value = 0.000005) and was responsible for 82.5% of the variation among the free energies. But while the cis and trans ligands, responsible for 46.8% of the variance in $\Delta G^{\ddagger}$,, played an impactful role in affecting relative free energies, the ligands themselves do not seem to have significantly differentiable impact on the catalyst performance (p-value = 0.147).

As the ANOVA test is omnibus, meaning that it does not have the capacity to differentiate the source of statistical significance within the specified groups, a Tukey HSD post-hoc analysis was run to compensate for this lack of information. We can see from the returned values of the evaluation in Table 2.5 that the statistically significant data is due to the “Chromium” subset of free energies while the “Tungsten” and “Molybdenum” subsets were not statistically different

enough to be considered a part of their own set (p-value = 0.202). Furthermore, the idea that the cis and trans ligands did not differ significantly is reinforced by this post-hoc analysis, which categorizes all the ligands in one subset.

III. CONCLUSION AND FUTURE WORK

This research investigates the thermodynamic affinity of an enzyme-based catalyst in assisting direct methane-to-methanol conversion, with emphasis on the barriers of C-H activation and ammonium involvement. We investigated a total of twenty-four reaction variations, modifying center metals (M = Cr, Mo, W), ethylene-dithiolate cis ligand R-groups (L_R= H, CH_3), and trans ligands (L_T = OH, CN, F, NO_3). From our relative free energy calculations, we found Cr-based catalysts to be the most thermodynamically favorable of all other catalyst structures in activating the inert C-H bond of methane. Analysis of average changes in relative free energies and C-C bond lengths over the reaction coordinate indicated little impact in varying the ethylene-dithiolate cis ligand R-groups, a discovery that contradicts expected dithiolene redox involvement [30]. Analysis of average changes in relative free energy indicated the trans ligand held some minor influence over catalyst performance. Thus, we can conclude the central metal played a significantly larger role in methane C-H bond activation than did cis or trans ligands. For transition-state metal complexes such as that modeled in this study, literature precedent supports the primary role of metal in functionalizing the inert C-H of methane by oxo complex [3, 15, 20].

This study also investigated the role of ammonium as a proton-donor. Across all reaction variants, we found an ammonium-involved pathway to be preferred over an ammonium-absent pathway in HAA intermediates. Ammonium-adduct formation in reactants varied based on each reaction, with no discernable pattern based on ligand or metal combinations. In ammonium-involved pathways, we observed the formation of ammonium adducts in reactants and HAA

intermediates, with some HAA intermediate pathways resulting in a full deprotonation of ammonium to form an aqua-complex.

Current results indicate that future works should delve deeper into the role a proton-donor such as ammonium plays in anionic metal complex performance, while also further investigating cis/trans ligand innocence. Experimentally, focus should be shifted to investigating the feasibility of chromium catalysts.

IV. REFERENCES

1. Božović, A., Feil, S., Koyanagi, G. K., Viggiano, A. A., Zhang, X., Schlangen, M., . . . Bohme, D. K. (2010). Conversion of Methane to Methanol: Nickel, Palladium, and Platinum (d9) Cations as Catalysts for the Oxidation of Methane by Ozone at Room Temperature. *Chemistry - A European Journal Chem. Eur. J., 16*(38), 11605-11610. doi:10.1002/chem.201000627

2. Božović, A., Feil, S., Koyanagi, G. K., Viggiano, A. A., Zhang, X., Schlangen, M., Schwarz, H. and Bohme, D. K. (2010), Conversion of Methane to Methanol: Nickel, Palladium, and Platinum (d9) Cations as Catalysts for the Oxidation of Methane by Ozone at Room Temperature. Chem. Eur. J., 16: 11605–11610. doi:10.1002/chem.201000627

3. Carsch, K. M., & Cundari, T. R. (2012). DFT modeling of a methane-to-methanol catalytic cycle via Group 6 organometallics: The role of metal in determining the mode of C–H activation. *Computational and Theoretical Chemistry, 980*, 133-137. doi:10.1016/j.comptc.2011.11.039

4. Olah, G. A. (2005), Beyond Oil and Gas: The Methanol Economy. Angewandte Chemie International Edition, 44: 2636–2639. doi:10.1002/anie.200462121

5. Wu, C., Yu, K. M., Liao, F., Young, N., Nellist, P., Dent, A., . . . Tsang, S. C. (2012). A non-syn-gas catalytic route to methanol production. *Nature Communications Nat Comms, 3*, 1050. doi:10.1038/ncomms2053

6. Periana, R. A. (1998). Platinum Catalysts for the High-Yield Oxidation of Methane to a Methanol Derivative. *Science, 280*(5363), 560-564. doi:10.1126/science.280.5363.560

7. Holmes, D. (2015). The problem with platinum. *Nature, 527*(7579). doi:10.1038/527s218a

8. Szaleniec, M., Witko, M., & Heider, J. (2008). Quantum chemical modelling of the C–H cleavage mechanism in oxidation of ethylbenzene and its derivates by ethylbenzene dehydrogenase. *Journal of Molecular Catalysis A: Chemical, 286*(1-2), 128-136. doi:10.1016/j.molcata.2008.02.016

9. Pavlov, M., Blomberg, M. R., Siegbahn, P. E., Wesendrup, R., Heinemann, C., & Schwarz, H. (1997). Pt -Catalyzed Oxidation of Methane: Theory and Experiment. *J. Phys. Chem. A The Journal of Physical Chemistry A, 101*(8), 1567-1579. doi:10.1021/jp962966w

10. Labinger, J. A., & Bercaw, J. E. (2002). Understanding and exploiting C–H bond activation. *Nature, 417*(6888), 507-514. doi:10.1038/417507a

11. Prince, B. M. (2014). The Mechanisms of Methane C–H Activation and Oxy-insertion Via Small Transition Metal Complexes: A DFT Computational Investigation (Doctoral dissertation, University of North Texas, 2014) (pp. 1-99). Denton, TX: UNT Theses and Dissertations.

12. Periana, R. A., Bhalla, G., Tenn, W. J., Young, K. J., Liu, X. Y., Mironov, O., . . . Ziatdinov, V. R. (2004). Perspectives on some challenges and approaches for developing the next generation of selective, low temperature, oxidation catalysts for alkane hydroxylation based on the CH activation reaction. Journal of Molecular Catalysis A: Chemical, 220(1), 7-25. doi:10.1016/j.molcata.2004.05.036

13. Teaw, S. L., Thornton, B. W., Qian, J., Jia, F., Pahls, D. R., & Cundari, T. R. (2015). DFT study of reductive functionalization in cis and trans cobalt–methyl–bipyridine complexes. Computational and Theoretical Chemistry, 1073, 102-105. doi:10.1016/j.comptc.2015.09.021

14. Fallah, H., & Cundari, T. R. (2015). Reductive functionalization of 3d metal–methyl complexes: The greater importance of ligand than metal. Computational and Theoretical Chemistry, 1069, 86-95. doi:10.1016/j.comptc.2015.06.011

15. Fallah, H., Horng, F., & Cundari, T. R. (2016). Theoretical Study of Two Possible Side Reactions for Reductive Functionalization of 3d Metal–Methyl Complexes by Hydroxide Ion: Deprotonation and Metal–Methyl Bond Dissociation. Organometallics, 35(7), 950-958. doi:10.1021/acs.organomet.5b00986

16. Marks, T. (n.d.). *Methane to Methanol What's Known and Questions/Challenges*. Lecture presented at NAS Workshop. Retrieved August 26, 2016.

17. M.J. Frisch et al., GAUSSIAN 09, Gaussian Inc, Wallingford, CT, 2009.

18. V.A. Rassolov, M.A. Ratner, J.A. Pople, P.C. Redfern, L.A. Curtiss
J. Comput. Chem., 22 (2001), pp. 976–984

19. A.V. Marenich, C.J. Cramer, D.G. Truhlar
J. Phys. Chem. B, 113 (2009), pp. 6378–6396

20. Lin, M., Shen, C., Garcia-Zayas, E. A., & Sen, A. (2001). Catalytic Shilov Chemistry: Platinum Chloride-Catalyzed Oxidation of Terminal Methyl Groups by Dioxygen. *J. Am. Chem. Soc. Journal of the American Chemical Society, 123*(5), 1000-1001. doi:10.1021/ja001926

21. Szaleniec, M., Hagel, C., Menke, M., Nowak, P., Witko, M., & Heider, J. (2007). Kinetics and Mechanism of Oxygen-Independent Hydrocarbon Hydroxylation by Ethylbenzene Dehydrogenase †. *Biochemistry, 46*(25), 7637-7646. doi:10.1021/bi700633c

22. Kalimuthu, P., Heider, J., Knack, D., & Bernhardt, P. V. (2015). Electrocatalytic Hydrocarbon Hydroxylation by Ethylbenzene Dehydrogenase from Aromatoleum

aromaticum. *The Journal of Physical Chemistry B J. Phys. Chem. B, 119*(8), 3456-3463. doi:10.1021/jp512562k

23. Kloer, D., Hagel, C., Heider, J., & Schulz, G. (2006). Crystal Structure of Ethylbenzene Dehydrogenase from *Aromatoleum aromaticum*. doi:10.2210/pdb2ivf/pdb

24. Evans, M. (2012, May 01). The trans/cis Effects & Influences. Retrieved September 17, 2016, from https://organometallicchem.wordpress.com/2012/05/01/the-transcis-effects-influences/

25. Dennington, R., Kieth, T., & Millam, J. (2009). GaussView 5. Retrieved September 17, 2015, from http://www.gaussian.com/g_prod/gv5.htm

26. Andrienko., G. A. (2004, August 8). Chemcraft - Graphical program for visualization of quantum chemistry computations. Retrieved October 20, 2015, from http://www.chemcraftprog.com/

27. Devore, J. L. (2016). *Probability and statistics for engineering and the sciences* (9th ed.). Boston, MA: Cengage Learning.

28. Hill, A. F., & Fink, M. J. (2011). *Advances in organometallic chemistry*. Oxford: Academic.

29. Kovacs, A.; Frenking, Gernot (2001). "Stability and Bonding Situation of Electron-Deficient Transition-Metal Complexes. Theoretical Study of the CO-Labilizing Effect of Ligands L in $[W(CO)_5L]$ (L = C_2H_2, NCH, N_2, C_2H_4, OH_2, SH_2, NH_3, F^-, Cl^-, OH^-, SH^-) and $[W(CO)_4L]^{2-}$ (L^{2-} = $O_2C_2H_2^{2-}$, $S_2C_2H_2^{2-}$) and the Structure of the 16-Valence-Electron Complexes $[W(CO)_4L]$ and $[W(CO)_3L]^{2-}$". *Organometallics*. **20** (12): 2510–2524. doi:10.1021/om0101893.

30. Eisenberg, R., & Gray, H. B. (2011). Noninnocence in Metal Complexes: A Dithiolene Dawn. *Inorg. Chem.*, 50(20), 9741-9751. doi:10.1021/ic2011748

31. Becke, A. D. (1993). A new mixing of Hartree–Fock and local density-functional theories. *The Journal of Chemical Physics J. Chem. Phys.*, 98(2), 1372. doi:10.1063/1.464304

32. Calculation of Vibrational Frequencies. (n.d.). Retrieved September 18, 2016, from http://openmopac.net/manual/vibrational_frequencies.html